

# Comparative Study of Central-Spin Entanglement and Coherence in Non-trivial Environment

Anushka Agrawal, Adithya A Vasista

*BITS Pilani, Hyderabad Campus*

---

## Abstract

We study an extended central spin model where two central qubits interact with a spin chain environment governed by a three-spin Ising Hamiltonian with periodic boundary conditions. Prior to introducing the central system, we examine static concurrence in the environment to identify signatures of quantum phase transitions. In the full model, we analyze entanglement dynamics under both equilibrium and non-equilibrium (quench) conditions. We find that entanglement generation is enhanced near criticality and is sensitive to the distance between central spins. The presence of three-spin interactions leads to key departures from integrable dynamics: (i) asymmetry under  $h \leftrightarrow -h$  quenches, (ii) enhanced entanglement near unconventional critical lines (e.g.,  $h = -J_3$ ), and (iii) delayed entanglement onset due to nonlinear quasiparticle dispersion. These results highlight the rich dynamical behavior arising from non-integrable interactions and offer insights into the interplay between criticality and entanglement generation in complex quantum systems.

---

## 1 Introduction

The study of entanglement is essential in the understanding of phase transitions and decoherence, thus playing a central role in Quantum Information and Many-Body Physics. The central spin model provides valuable insights into the generation and evolution of entanglement in the central spins and the effects of interaction with the bath environment. This work explores the working of an extended central spin model, consisting of initially separable central spins, coupled to a spin chain environment with a periodic boundary. The environment is governed by the non-integrable three-spin Ising Hamiltonian, which has been proposed for experimental realization in optical lattices Ref.<sup>[12]</sup>.

Before we delve into the working of the system

in the presence of the central spin, we will establish signatures of criticality by analyzing concurrence. Further introduction of the central spins is done in order to understand entanglement behavior in a previously separable state by studying both equilibrium and quench dynamics.

From the above-discussed study, we discover that entanglement increases near critical boundaries and has a long order in the equilibrium regime. As we move to the dynamic study, critical quenches lead to peaking of entanglement. The presence of the three-spin interactions in the bath gives rise to distinctive features: symmetry breaking under  $h \leftrightarrow -h$  quenches, and unconventional peaks at critical lines (e.g.,  $h = -J_3$ ) as seen from the phase diagram.

---

## 2 Phase Transition and Entanglement

## 2.1 3-Spin-Ising model

The Hamiltonian for the three-spin interacting Ising model is given by:

$$H = -\frac{1}{2} \left\{ \sum_i \sigma_i^z [h + J_3 \sigma_{i-1}^x \sigma_{i+1}^x] + J \sum_i \sigma_i^x \sigma_{i+1}^x \right\}$$

where  $h$  is the transverse field,  $J_3$  is the strength of the three-spin interaction, and  $J$  controls the nearest-neighbor coupling.

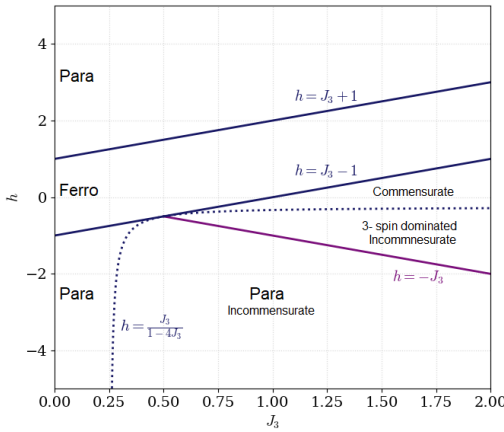


Figure 1: Equilibrium phase diagram of the three-spin interacting Ising model. Solid lines show phase boundaries, and the dotted line marks the boundary between the incommensurate and commensurate phases.

We define the three-spin Ising Hamiltonian as shown above. The term with  $J_3$  introduces next-nearest-neighbor effects through a three-body interaction, modifying the critical behavior compared to the standard transverse field Ising model (TFIM) Ref. [14].

To analyze the Hamiltonian, we apply the Jordan–Wigner transformation to map the spin operators to fermionic operators. The transformation is defined as:

$$c_i^\dagger = \sigma_i^+ \exp \left( -i\pi \sum_{j=1}^{i-1} \sigma_j^z \right)$$

$$\sigma_i^x = 2c_i^\dagger c_i - 1$$

$$c^\dagger = \frac{\sigma^x + i\sigma^y}{2}, \quad c = \frac{\sigma^x - i\sigma^y}{2}, \quad (1)$$

which satisfy the standard fermionic anti-commutation relations:

$$\{c_i^\dagger, c_j\} = \delta_{ij}, \quad \{c_i^\dagger, c_j^\dagger\} = \{c_i, c_j\} = 0.$$

We diagonalize the Hamiltonian using the Jordan–Wigner transformation, converting spins into fermions. We work in the basis where  $\sigma^z$  is diagonal, such that the presence of a fermion at site  $i$  corresponds to an up spin ( $\sigma_i^z = +1$ ) at that site. This allows us to analyze the system in momentum space using standard fermionic techniques. Under periodic boundary conditions, we can Fourier transform the Hamiltonian. The resulting expression, derived following Ref. [3].

$$H = - \sum_{k>0} (h + \cos k - J_3 \cos 2k)(c_k^\dagger c_k + c_{-k}^\dagger c_{-k}) + i(\sin k - J_3 \sin 2k)(c_k^\dagger c_{-k}^\dagger + c_{-k} c_k)$$

$$H = - \sum_k \epsilon_k \eta_k^\dagger \eta_k,$$

In the momentum basis, the Hamiltonian is quadratic in fermionic operators and exhibits translational invariance. It can be diagonalized using a Bogoliubov transformation: Where,  $\eta_k$  are the Bogoliubov quasiparticles and  $\epsilon_k$  is the excitation energy or gap given by:

$$\epsilon_k = \sqrt{h^2 + 1 + J_3^2 + 2h \cos k - 2h J_3 \cos 2k - 2J_3 \cos k} \quad (2)$$

with  $J$  set equal to unity.

It can be shown that the gap of the spectrum vanishes at  $h = J_3 + 1$  and also at  $h = J_3 - 1$  with ordering (or mode-softening) wave vectors  $\pi$  and  $0$ , respectively. These two lines correspond to quantum phase transitions from

a ferromagnetically ordered phase to a quantum paramagnetic phase, with associated exponents being the same as the transverse Ising model. The wave vector at which the minima of  $\epsilon_k$  (Eq. 4) occur, shifts from  $k = 0$  to  $k = \pi$  wave vector when one crosses the line  $h = J_3$ . Moreover, there is an additional phase transition at  $h = -J_3$ . This transition belongs to the universality class of the anisotropic transition observed in the transverse XY-model.

## 2.2 Concurrence

Concurrence is a widely used measure to quantify entanglement in a two-qubit system. For a pair of spins described by a mixed state density matrix  $\rho$ , the concurrence  $C(\rho)$  Ref. [16] is computed using the following procedure:

1. Construct the spin-flipped state:

$$\tilde{\rho} = (\sigma_y \otimes \sigma_y)\rho^*(\sigma_y \otimes \sigma_y)$$

$\rho^*$  here is the conjugate of  $\rho$  the density matrix

2. Forming the hermitian matrix R:

$$R = \sqrt{\sqrt{\rho}\tilde{\rho}\sqrt{\rho}}$$

3. Calculate the eigenvalues  $\lambda$  of the R and sort them from highest to lowest such that

$$\lambda_1 > \lambda_2 > \lambda_3 > \lambda_4$$

$$C(\rho) = \max(0, \lambda_1 - \lambda_2 - \lambda_3 - \lambda_4)$$

Since concurrence is defined only for two-qubit systems, we reduce the full many-body density matrix to a  $4 \times 4$  reduced density matrix by tracing out the environmental degrees of freedom. This is done using the ground-state wavefunction of the Ising Hamiltonian. To isolate entanglement between a specific spin pair, we compute the reduced density matrix

by tracing over all other lattice sites. This allows us to evaluate the concurrence between selected sites in the chain.

\*

## Identifying Phase Transitions

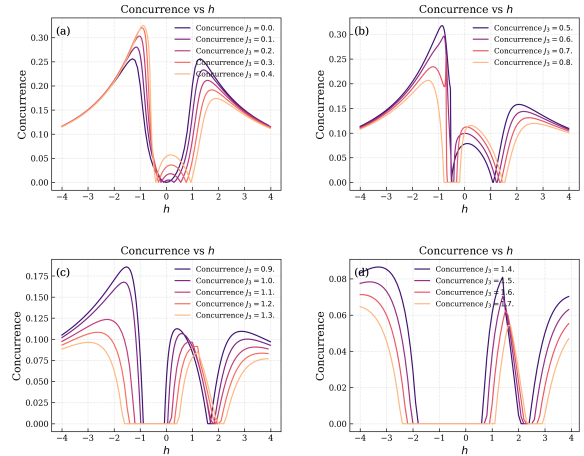


Figure 2: Plot for Concurrence ( $C$ ) as a function of Transverse Field ( $h$ ) for  $J_3 = 0$  to 1.7

We analyze quantum phase transitions through the lens of entanglement by examining concurrence as a function of the transverse field  $h$ . The concurrence exhibits pronounced peaks at specific values of  $h$ , which correspond to critical points in the system's phase diagram.

In Fig. 2 (a), for  $J_3 = 0$ , the concurrence reaches a maximum near  $h \approx \pm 1$ , consistent with the critical points of the Transverse Field Ising Model. Once three-spin interaction is introduced through  $J_3$ , the peaks of Transverse Field Ising shift to  $h = J_3 + 1$  and  $h = J_3 - 1$ , and we also see a small peak corresponding to  $h = \frac{J_3}{1-4J_3}$ . As  $J_3$  increases, when  $J_3 > 0.5$  Fig.2 (b), the concurrence peak shifts to  $h = -J_3$ , which follows the phase diagram. The region between these peaks shows a drastic drop in concurrence, which is expected in a phase transition where the entanglement

\*We study concurrence as a function of the transverse field  $h$  instead of the ratio  $\lambda = J/h$  used in Ref. [10]. In our three-spin Ising model, this approach allows for a clearer identification of phase boundaries, especially in regions with commensurate and incommensurate order, and aligns better with critical points in our extended parameter space.

structure changes, and the concurrence is completely 0, in the 3-spin-dominated incommensurate state, and the Commensurate state. This is very evident in Fig. 2(d), where this region is only noticeable when  $J_3 > 0.5$ , which is a clear indication of the expected behavior from the phase diagram. We also observe that the critical point corresponding to  $h = J_3 - 1$  starts shifting towards the positive  $h$  which is evident from Fig. 2(c) and Fig. 2(d). The phase diagram Fig. 2 shows phase boundaries at:

$$\begin{aligned} h &= 1 + J_3 \\ h &= J_3 - 1 \\ h &= -J_3 \\ h &= \frac{J_3}{1 - 4J_3} \end{aligned}$$

The concurrence plots serve as indirect detectors of quantum phase transitions. As we vary  $h$ , we observe distinct entanglement signatures that align with known critical lines, as well as possible emergent structures not visible in the energy gap alone. Which was very well established in Ref. [10;9].

Comparing the concurrence peaks with the analytically predicted phase boundaries, we find strong agreement. This reinforces the idea that entanglement measures can serve as robust probes of quantum criticality, even in models with non-trivial interactions like the three-spin Ising chain.

### 3 Central Spin

#### Locally coupling two independent spins to a one-dimensional spin chain

##### 3.1 Modeling the Hamiltonian

We extend the traditional central spin model by introducing two non-interacting central spins, each locally coupled to a one-dimensional spin chain that acts as the environment. The environment can follow either the longitudinal field Ising model or the three-spin Ising model. Our goal is to investigate how these environmental settings affect entanglement generation, especially under non-equilibrium conditions induced by a sudden quench of the transverse field.

We consider a generalized central spin model GCSM in which two non-interacting local interaction connects spins to an environmental spin chain, chosen to be a one-dimensional ferromagnetic Ising spin model, in such a way that the local transverse field of the environmental spin chain gets modified. The composite system, thus, is a GCSM, in which a single spin-1/2 particle Ref. [13] is globally connected to all the spins of the environmental spin chain with an interaction Hamiltonian.

The schematic diagram of the GCSM is shown. The combined Hamiltonian  $H_T$ , comprising an environmental transverse Ising Hamiltonian  $H_E$  with  $N$  spins and interaction Hamiltonian  $H_{SE}$  of two spins is given by:

$$H_T = H_{SE} + H_E$$

We consider a PBC,  $\sigma_{N+1}^i = \sigma_1^i$ . The interaction Hamiltonian takes the form:

$$H_{SE} = -\delta(|\uparrow\rangle\langle\uparrow|_A \otimes \sigma_p^z + |\uparrow\rangle\langle\uparrow|_B \otimes \sigma_q^z);$$

where  $A$  and  $B$  denote the two central spins, and  $p$  and  $q$  are their respective coupling sites on the chain, separated by a distance  $d = |p - q|$ . The parameter  $\delta$  controls the interaction strength. Where,  $|\uparrow\rangle_{AB}$  is an eigenstate of operator  $\sigma_{A,B}^z$  satisfying the relation  $\sigma_{A,B}^z |\uparrow\rangle_{A,B} = |\uparrow\rangle_{A,B}$ .

We typically consider the weak-coupling limit  $\delta \rightarrow 0$ , where the central spins minimally disturb the environment but still influence its dynamics. The interaction Hamiltonian  $H$  in

the equation indicates that coupling with the central spins alters the local transverse field of the environment. To study entanglement generation, we initialize the system in a completely unentangled product state of the two central spins:

$$|\phi\rangle_{AB} = \frac{1}{2}(|\uparrow\rangle_A + |\downarrow\rangle_A) \otimes (|\uparrow\rangle_B + |\downarrow\rangle_B) \quad (3)$$

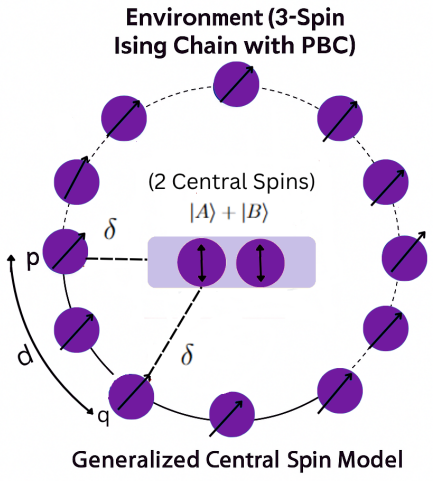


Figure 3: Illustration explaining CSMs

Our current study focuses on the non-equilibrium or quenching Ref. [7] condition by quantifying the change under temporal evolution in the composite system entanglement due to an instantaneous change in the parameter  $h$ , transverse field strength (from  $h_i$  to  $h_f$ ). At equilibrium we have  $h_i = h_f$ , and the initial state can be written as

$|\psi\rangle(h_i, t = 0) = |\phi\rangle_{A,B} \otimes |\eta\rangle(h_i, t = 0)$  Depending on the configuration of the two central spins, the environment evolves under one of four Hamiltonians and  $h_f$  governs the evolutionary dynamics  $H_{\alpha\beta}$  given by:

$$\begin{aligned} H_{\downarrow\downarrow}(h_f) &= H_E(h_f) \\ H_{\uparrow\uparrow}(h_f) &= H_E(h_f) - \delta(\sigma_p^z + \sigma_q^z) \\ H_{\uparrow\downarrow}(h_f) &= H_E(h_f) - \delta(\sigma_p^z) \\ H_{\downarrow\uparrow}(h_f) &= H_E(h_f) - \delta(\sigma_q^z) \end{aligned}$$

This gives us the time-evolved state as:

$$\begin{aligned} |\psi\rangle = \frac{1}{2}(&|\uparrow\uparrow\rangle \otimes \eta_{\uparrow\uparrow}(t) + |\downarrow\downarrow\rangle \otimes \eta_{\downarrow\downarrow}(t) \\ &+ |\uparrow\downarrow\rangle \otimes \eta_{\uparrow\downarrow}(t) + |\downarrow\uparrow\rangle \otimes \eta_{\downarrow\uparrow}(t)) \quad (4) \end{aligned}$$

To time evolve the states with our time-independent Hamiltonians, the initial ground state without modified Hamiltonians is exponentiated using the 4 different Hamiltonians created above: where  $\alpha\beta$  in  $|\eta_{\alpha\beta}(t)\rangle$  represents the state of the two spins.

$$|\eta_{\alpha\beta}(t)\rangle = e^{-iH_{\alpha\beta}t} |\eta(h_i, t = 0)\rangle \quad (5)$$

The  $h_i = h_f$  for the equilibrium study. The reduced density matrix is constructed by tracing out environmental degrees of freedom. The matrix for the system of two spins is shown below:

$$\rho_s(t) = \frac{1}{4} \begin{bmatrix} 1 & |d_{\uparrow\uparrow,\uparrow\downarrow}| & |d_{\uparrow\uparrow,\downarrow\uparrow}| & |d_{\uparrow\uparrow,\downarrow\downarrow}| \\ |d_{\uparrow\uparrow,\uparrow\downarrow}| & 1 & |d_{\downarrow\downarrow,\uparrow\downarrow}| & |d_{\downarrow\downarrow,\downarrow\downarrow}| \\ |d_{\uparrow\uparrow,\downarrow\uparrow}| & |d_{\downarrow\downarrow,\uparrow\downarrow}| & 1 & |d_{\downarrow\downarrow,\downarrow\downarrow}| \\ |d_{\uparrow\uparrow,\downarrow\downarrow}| & |d_{\downarrow\downarrow,\downarrow\downarrow}| & |d_{\downarrow\downarrow,\uparrow\downarrow}| & 1 \end{bmatrix}$$

The  $d_{\alpha\beta,\lambda\gamma}$  terms are obtained from the inner product of the various terms  $\langle \eta_{\lambda\gamma} | \eta_{\alpha\beta} \rangle$  and the echoes corresponding to this calculation can be found using  $D_{\alpha\beta\gamma\lambda}(t) = |d_{\alpha\beta,\lambda\gamma}|^2$

We use this density matrix as shown above to calculate the concurrence values for the benchmark [6], as well as the plots and inferences that we will develop in the paper.

Before presenting our new study, we first demonstrate the effectiveness of Exact Diagonalization, despite its limitation to small system sizes from Ref. [5]. We show that it can reproduce results with remarkable accuracy, closely matching those obtained using other established methods such as the Jordan-Wigner transformation Ref. [11] (for exactly solvable systems) and the Density Matrix Renormalization Group (DMRG) Ref. [2], which, can handle much larger system sizes.

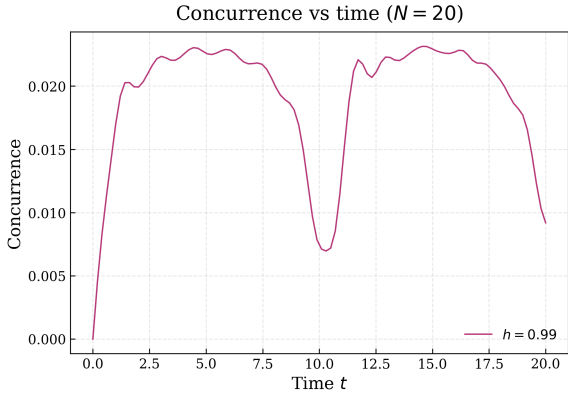


Figure 4: Plot capturing dip at  $t = \frac{N}{2}$

FIG. 4 demonstrates that our exact diagonalization method reproduces known results from Ref. [6] using Exact Diagonalization, with high fidelity, validating our approach for the chosen system size and parameters ( $h_i = h_f = 0.99$ ), to benchmark our method near the critical point for the infinite lattice.

The concurrence exhibits non-trivial, revival-like dynamics near the critical point, consistent with expectations from Ref. [6]. While the overall behavior resembles that of larger systems, finite-size effects introduce subtle differences. The concurrence oscillations observed for our finite system size are qualitatively similar to those seen in larger-scale studies.

### 3.2 Three-Spin Ising model

As discussed previously, the Hamiltonian corresponding to the three spin Ising model is mentioned below. Ref. [7;8].

$$-\frac{1}{2} \left\{ \sum_i \sigma_i^z [h + J_3 \sigma_{i-1}^x \sigma_{i+1}^x] + J \sum_i \sigma_i^x \sigma_{i+1}^x \right\}$$

We will be discussing the 3-spin model in the light of equilibrium and dynamic study using exact diagonalization with the additional central spin term in this section.

#### 3.2.1 Equilibrium Study

The equilibrium case corresponds to  $h_i = h_f$ , where the environment evolves under a con-

stant field. Depending on the initial configuration of the central spins, the system follows one of four environmental evolution channels. We first focus on studying the central spin dynamics at the environmental quantum critical points, starting with the critical point.

$$h \approx (1 + J_3)$$

In the absence of the three-spin term, previous studies (Ref. [6]) have reported a characteristic dip in concurrence at  $t = \frac{N}{v}$ . This arises due to constructive interference of quasiparticles with group velocity  $v = 2$ .

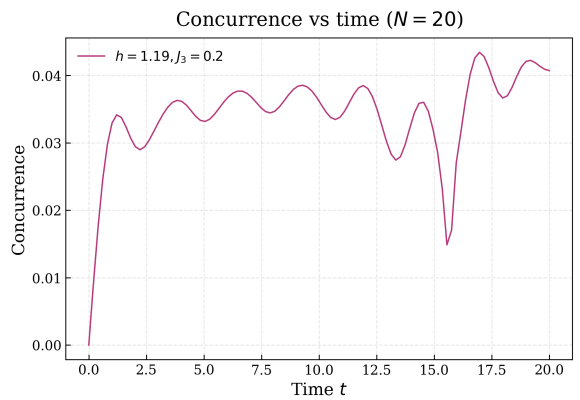


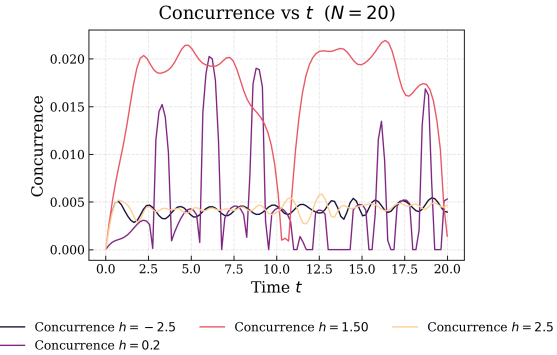
Figure 5: Equilibrium  $h_i = h_f = 1.19$

This plot corresponds to  $J_3 = 0.2$  with  $h_i = h_f = 1.19$ . Unlike the integrable TFIM case, no sharp dip is observed at  $t = N/2$ , indicating that such dips are not universal signatures of criticality. In the three-spin Ising model, large  $J_3$  values lead to nonlinear dispersion and quasiparticles propagating at different velocities. To estimate the dip time in concurrence, we compute the maximum group velocity  $v_{\max}(J_3)$  from the dispersion relation (Eq. 2), and use:

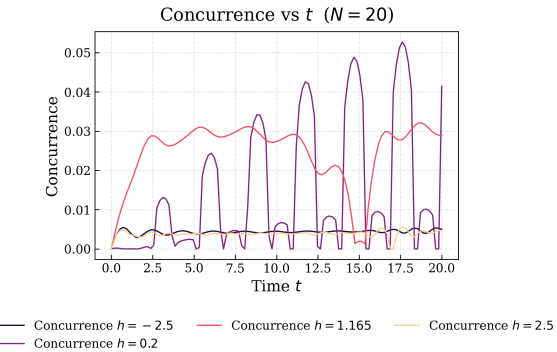
$$t_{\text{dip}} \approx \frac{N}{v_{\max}(J_3)}$$

For each value of  $J_3$ , we evaluate  $v_{\max}$  and estimate the corresponding dip time using the above relation. In the three-spin Ising model, increasing the interaction strength  $J_3$  leads to a progressive suppression of the concurrence dip at  $t_{\text{dip}}$  (for  $d = 0$ ). This indicates the breakdown of coherent quasiparticle interference due

to the onset of non-integrability. As  $J_3$  grows, the dispersion becomes increasingly nonlinear, intermode scattering intensifies, and parity-breaking effects degrade long-range coherence. As a result, the sharp dip characteristic of the integrable TFIM is smoothed out, marking a transition from coherent ballistic to incoherent dynamics. This highlights the sensitivity of entanglement features to the interaction structure of the environment.



(a) Equilibrium plot for  $N = 20$   $J_3 = 0.5$  for multiple values of  $h$



(b) Equilibrium plot for  $N = 20$   $J_3 = 0.165$  for multiple values of  $h$

Figure 6: Time evolution of concurrence  $C(t)$  at critical points corresponding to  $h = 1 + J_3$ .

**(a)** For  $J_3 = 0.5$ ,  $h_i = h_f = 1.5$ , a sharp dip is observed at  $t = N/2$ , consistent with coherent quasiparticle interference and linear dispersion with group velocity  $v_{\max} = 2$ . **(b)** For  $J_3 = 0.165$ ,  $h_i = h_f = 1.165$ , the concurrence dip occurs near  $t \approx 15$ , corresponding to  $v_{\max} \approx 1.33$ . These results illustrate how the dip time in concurrence reflects the group velocity of quasi-particles in the three-spin Ising environment.

At criticality ( $h = 1 + J_3$ ), a sharp dip appears in the concurrence due to coherent quasiparticle interference and well-defined group velocities near linear dispersion. In the Paramagnetic phase ( $h = \pm 2.5$ ), the concurrence shows smooth, similar behaviour for both signs of  $h$ ; no distinct features emerge due to the presence of a gapped excitation spectrum, and concurrence remains mostly constant for a long period. In the Ferromagnetic phase ( $h = 0.2$ ), concurrence exhibits oscillatory behavior with larger amplitude, indicating the existence of a more robust entanglement channel supported by the ordered ground state. Interestingly, the dip time,  $t_{\text{dip}}$  aligns with a ballistic light-cone-like spreading of entanglement, reminiscent of the Lieb-Robinson bound Ref. [4]. While our model is non-integrable, a well-defined group velocity still governs early-time entanglement spread.

### 3.3 Finite-Size Scaling

In the vicinity of the critical point, observables like concurrence exhibit behaviors independent of system size. This behavior is characterized by power-law scaling and is governed by critical scaling exponents.

To analyze the scaling behavior of the dip value of concurrence  $C_{\text{dip}}$  with system size  $N$ , we plot the normalized values  $C_{\text{dip}}/C_{\max}$  against  $1/N$  on a log-log scale. A linear fit is performed to the logarithmically transformed data, yielding a power-law behavior of the form

$$C_{\text{dip}} \propto \left(\frac{1}{N}\right)^{\alpha},$$

This behavior suggests that the dip in concurrence scales sub-extensively with system size and may vanish in the thermodynamic limit. The extrapolated value of  $C_{\text{dip}}$  as  $N \rightarrow \infty$  is consistent with zero (or finite value ( $C_{\infty} = 0$ ), depending on intercept). The curves for different  $N$  values will all collapse onto a single curve near this point. This scaling acts as evidence that the entanglement dynamics re

are sensitive to quantum criticality, as used in Ref. [15]

### 3.4 Dynamic Study

We note that in the Dynamic study, unlike the equilibrium study,  $h_i$  and  $h_f$  are not equal. We are going to extend our previous equilibrium study, the environmental spin chain undergoes global sudden quenching, by which we mean to say that the transverse field  $h_i$  is suddenly changed to  $h_f$ , based on the previous study conducted Ref. [6], we see how concurrence evolves and how strongly the system gets correlated for multiple values of  $J_3$  and  $h_i$ , keeping  $h_f$  constant at 2.2 for the next plot.

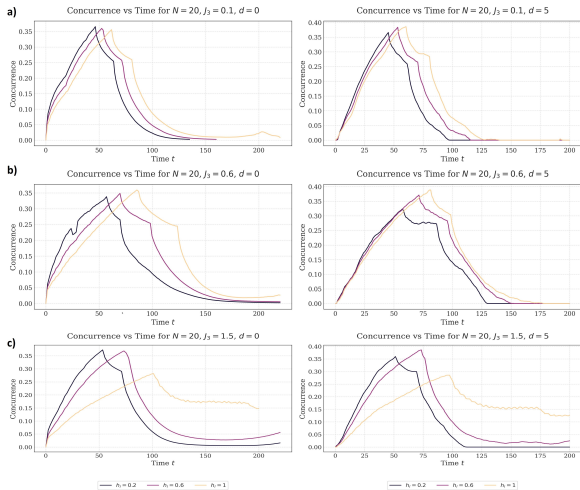


Figure 7: Concurrence dynamics for different three-spin interaction strengths  $J_3$  under a quench to  $h_f = 2.2$ . **(a)** For  $J_3 = 0.1$ , concurrence shows a sharp peak and rapid decay, indicating near-integrable, ballistic behavior. **(b)** For  $J_3 = 0.6$ , the growth is slower with broader peaks and delayed decay. **(c)** For  $J_3 = 1.5$ , the dynamics become flatter and less structured, reflecting strong dephasing and incoherence at high non-integrability.

At weak three-spin coupling ( $J_3 = 0.1$ ), the concurrence between central spins rises sharply, reaches a well-defined peak, and rapidly decays. The decay is more pronounced for lower initial field values  $h_i$ , indicating enhanced dephasing

in the presence of a more ordered environment. The overall dynamics resemble ballistic entanglement spreading typically observed in near-integrable systems, where quasiparticles propagate coherently and interfere constructively over short timescales.

As the three-spin coupling increases to moderate values (e.g.,  $J_3 = 0.6$ ), the behavior becomes qualitatively different. The growth of concurrence is noticeably slower, the peak broadens, and the decay becomes more gradual. The introduction of frustration via higher  $J_3$  disrupts coherent quasiparticle motion, slowing down the buildup of entanglement and simultaneously extending its temporal lifetime. Weak revival-like oscillations emerge at late times, likely arising from competing modes and residual interference patterns in a weakly non-integrable background.

At even larger  $J_3$ , the system enters a deeply non-integrable regime, where ballistic spreading is strongly suppressed, and the concurrence profile becomes flatter with overall reduced peak height. The entanglement dynamics become increasingly dominated by incoherent processes, reflecting the absence of well-defined quasiparticle trajectories. We observe that the concurrence peak decreases and the concurrence exhibits a longer revival time when quenching from  $h_i = 1$ , as shown in Fig. 7(c). This behavior is attributed to the fact that both the initial field  $h_i$  and the final quenching field  $h_f$  belong to the same phase for  $J_3 = 1.5$ , as illustrated in Fig. 1.

This transition from rapid, coherent entanglement growth to slower, dephased dynamics as a function of  $J_3$  highlights the rich structure of non-equilibrium behavior in the three-spin Ising environment. A more detailed analysis of these effects—including the identification of distinct dynamical regimes, thresholds for entanglement revival, and the role of initial conditions—is presented in the upcoming Sec. 3.5.

### 3.4.1 Asymmetry in Entanglement under Field Reversal

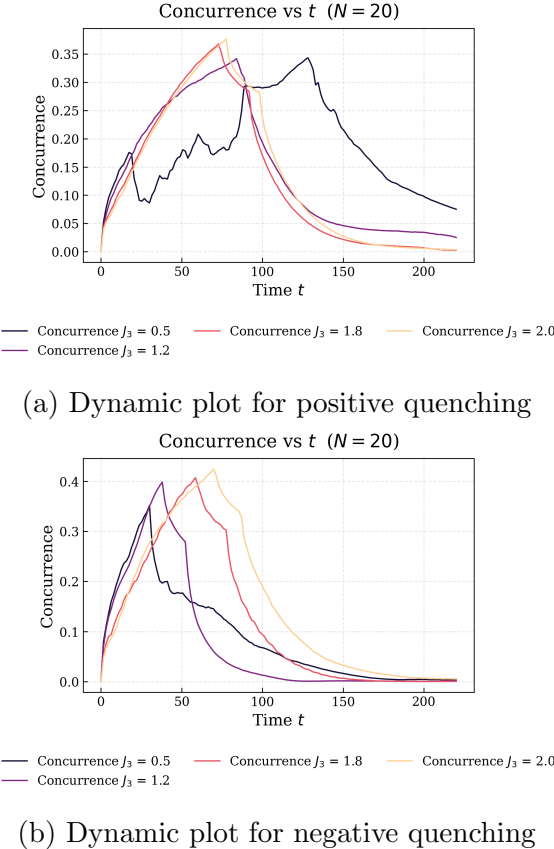


Figure 8: (a) For  $h_f = 1.5$ , the concurrence exhibits a moderate peak around 0.35, followed by a rapid decay. (b) For  $h_f = -1.5$ , the concurrence reaches a higher peak of approximately 0.4 and decays more slowly. This asymmetry in entanglement dynamics reflects the broken  $h \leftrightarrow -h$  symmetry of the three-spin Ising model.

The three-spin Ising Hamiltonian is typically of the form:

$$-\frac{1}{2} \left\{ \sum_i \sigma_i^z [h + J_3 \sigma_{i-1}^x \sigma_{i+1}^x] + J \sum_i \sigma_i^x \sigma_{i+1}^x \right\}$$

The transverse field  $h$  couples linearly to  $\sigma^x$ , but the three-spin term involves mixed components like  $\sigma^z \sigma^x \sigma^x$ , which does not respect a simple  $h \rightarrow -h$  symmetry.

As a result, the spectrum and eigenstates of

the Hamiltonian are generally not symmetric under  $h \leftrightarrow -h$ .

One key observation is that the concurrence peak for  $h < 0$  is consistently greater than that for  $h > 0$ . This asymmetry arises due to the presence of a new quantum critical point  $h = -J_3$ , introduced by the three-spin interaction term. As shown in Fig. 2, where the central spin is absent, entanglement is generally enhanced for negative transverse fields. This asymmetric behavior, where entanglement is enhanced for negative values of  $h$ , appears to be a robust feature of the system and is consistent across various parameter regimes. This trend becomes even more apparent in the heatmap plots presented in the following section 3.5, further supporting the universality of this entanglement enhancement under field inversion due to the additional critical point at  $h = -J_3$ .

### 3.4.2 Intra-Phase Quenching

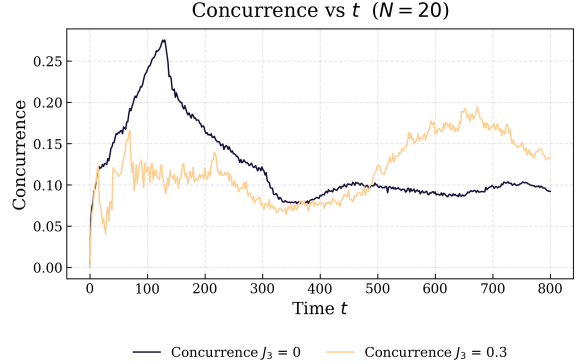
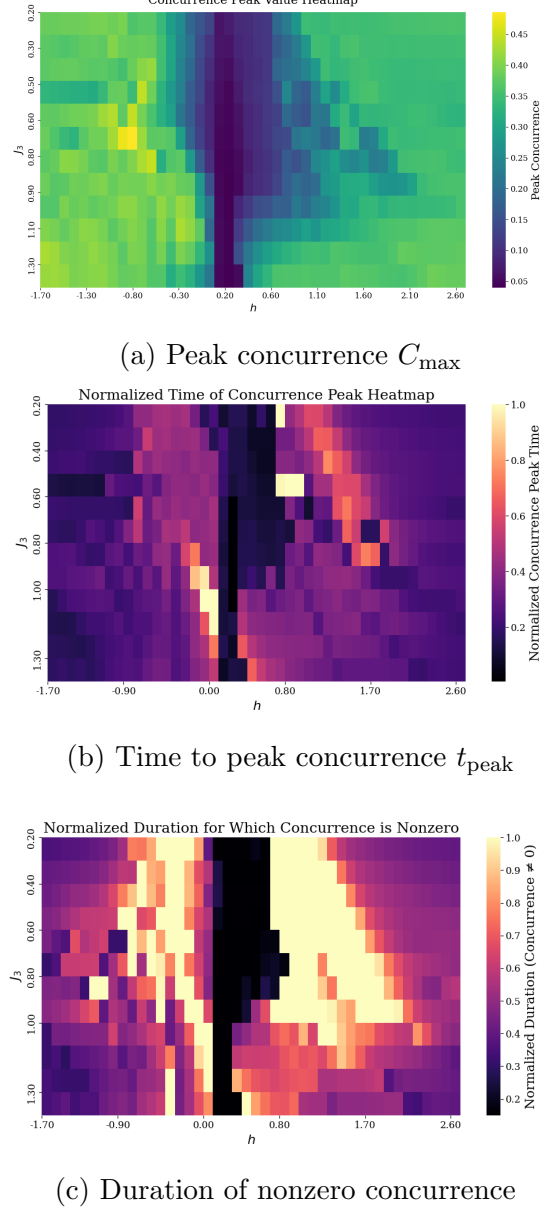


Figure 9: Time evolution of concurrence  $C(t)$  between two central spins for  $N = 20$  under a quench  $h_i = 0.2, h_f = 0.7$ , at various three-spin interaction strengths  $J_3$

In Fig. 9, the parameter  $J_3$ , representing the strength of the three-spin interaction, fundamentally alters the entanglement dynamics between central spins. The behavior of the concurrence dynamics is highly dependent on the quenching path. We see longer-lasting concurrence if the quenching field ( $h_f$ ) is in the same phase as the initial field ( $h_i$ )

At small  $J_3$ , the system retains near-integrable behavior almost similar to the TFIM. In this regime, quasiparticle excitations generated by the quench produce smooth, long-lived oscillations in the concurrence, reflecting interference effects and delayed entanglement revival. Here, we see that  $J_3$  plays a major role if we want the system to stay entangled for a long period, we observe that the standard TFIM has an early primary peak and shows a slow decay, but the introduction of  $J_3$  helps retain the concurrence for long period of time.



### 3.5 Dynamical Landscape of Central Spin Entanglement

To obtain a global perspective on the entanglement behavior, we construct dynamical phase diagrams using concurrence data sampled across a broad range of transverse field values  $h$  and three-spin interaction strengths  $J_3$ . These diagrams offer a statistical and time-resolved overview of how central spin entanglement evolves throughout the parameter space, highlighting regions of enhanced quantum correlations and revealing the interplay between integrability and non-integrability in the system.

Figure 10: Composite figure showing various dynamical properties of central spin concurrence: (a) Heatmap of the peak concurrence as a function of the transverse field  $h$  and three-spin interaction  $J_3$ . For  $h_i = 0.2$ , (b) Heatmap of the normalized time at which concurrence reaches its peak. (c) Heatmap of the normalized duration for which the concurrence remains nonzero during time evolution, and these plots together characterize the temporal and spatial structure of entanglement in the parameter space  $(h, J_3)$ .

Fig. 10(a) shows the maximum value of the agreement observed during time evolution for

each pair  $(h, J_3)$ . The heatmap reveals regions of enhanced entanglement generation, with high concurrence values clustering around critical points. In particular, the asymmetry under  $h \leftrightarrow -h$  is evident, especially at intermediate values of  $J_3$ , consistent with the parity-breaking nature of the three-spin interaction. Interestingly, a strong entanglement “ridge” is visible near  $h \approx -J_3$ , indicating critical enhancement in that region. A bright blue patch is observed in the region  $h \in [0.2, 0.4]$ , indicating almost no concurrence, which is consistent with the equilibrium study. We observe a darker greenish-blue patch along the diagonal in the range  $h \in [0.3, 2.1]$ , which corresponds to intra-phase quenches. In this region, the concurrence peak is comparatively suppressed, indicating weaker entanglement enhancement relative to other parameter regimes.

Figure 10(b) illustrates the normalized time at which the concurrence reaches its maximum. This time-resolved analysis provides insight into the quasiparticle propagation dynamics. Peaks occurring at later times (brighter regions) are indicative of delayed entanglement due to slower group velocities or complex interference effects. Regions with early entanglement generation appear dark, matching expectations from dynamics. We also observe a clear delay in the concurrence peak time along the same diagonal, where the peak value is suppressed. This again indicates intra-phase quenching, which hinders rapid entanglement generation.

To probe the persistence of entanglement, we plot in Fig. 10(c) the normalized duration for which concurrence remains nonzero during time evolution. This quantity captures how long the central spins stay entangled. Extended durations are observed in wide parameter ranges, particularly when  $h \in [0.5, 1.8]$  and for moderate  $J_3$ . The dark vertical stripe near  $h = 0.2$  this region corresponds to near-vanishing concurrence, suggesting an environment dominated by strong decoherence or suppressed correlations, as expected from equilib-

rium considerations. This behavior is consistent with the decoherence analysis presented in Sec. 3.6, which provides deeper insight into the observed delay in entanglement generation in both equilibrium and quench dynamics.

These figures provide a dynamical phase-space characterization of entanglement in the central spin model. By combining spatial, temporal, and statistical perspectives, this analysis helps uncover which regions of the parameter space are most favorable for robust and long-lived entanglement.

### 3.6 Analysis Through Decoherence Channels

In this section, we shall analyze the results presented in the previous sections using the decoherence factor (DF), or equivalently, the Loschmidt echo (LE) associated with distinct decoherence channels (DCs), which in turn leads to the generation associated with the different DCs and the spins, which are initially unentangled. The  $D_{\alpha\beta\gamma\lambda}(t)$  term, as calculated above, is used to quantify decoherence. The quantification of the information lost to the system is done using this quantity in our study. When we add the  $J_3$  term to the system, it alters the entanglement growth. To analyze how this impacts decoherence, we utilize the Loschmidt Echo. The echo parameterizes how fast the information is lost and for how long the entanglement will last. The quantity is found to be the square of the decoherence factor that we have already seen in the previous sections and is given as:

$$L(t) = |D_{\alpha\beta\gamma\lambda}(t)|^2 = |d_{\alpha\beta,\lambda\gamma}|^4 \quad (6)$$

First, we analyze decoherence for multiple plots.

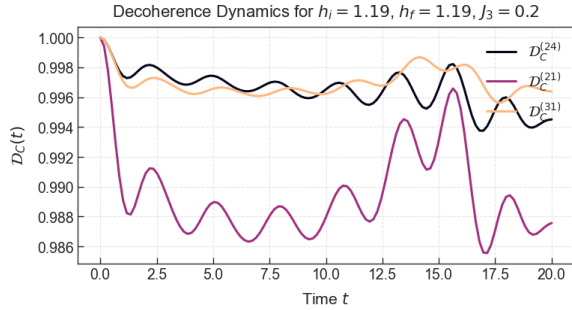


Figure 11: Decoherence for equilibrium study  
 $h_i = h_f = 1.19$

This plot corresponds to Fig. 5, we see a peak in decoherence right when there is a dip in concurrence.

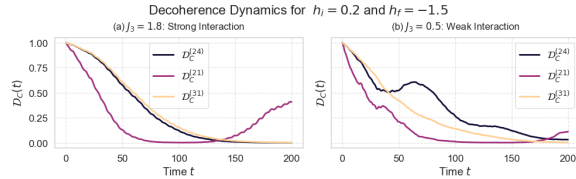


Figure 12: Decoherence for Dynamic study  
 $h_i=0.2$   $h_f=-1.5$

## 4 Conclusions

In this work, we studied a central spin model with two qubits coupled to a three-spin interacting spin chain. Using exact diagonalization, we analyzed entanglement generation both in equilibrium and following quenches of the transverse field.

Our results demonstrate that quantum criticality in the environment plays a crucial role in enhancing and sustaining entanglement. We showed that time-averaged concurrence peaks near critical  $J_3$  values, and the dynamic behavior exhibits clear asymmetries due to the lack of  $h \leftrightarrow -h$  symmetry in the model.

These findings indicate that environmental phase transitions can serve as entanglement amplifiers in spin-chain-mediated quantum systems, with potential applications in quantum information protocols where tunable entanglement is needed.

## References

- [1] Kevin Ann and Gregg Jaeger. Disentanglement and decoherence in two-spin and three-spin systems under dephasing. *Phys. Rev. B*, 75:115307, Mar 2007.

**Fig. 12:** Decoherence dynamics  $D_C(t)$  for different coupling channels at (b)  $J_3 = 0.5$  and (a)  $J_3 = 1.8$ . Correspond to the dynamic concurrence study Fig. 8b. The curves represent distinct environmental evolutions associated with different central spin configurations. At weak coupling, decoherence is slower and exhibits revivals due to quasiparticle interference, while at strong coupling, decoherence becomes faster and smoother, indicating non-integrable dynamics. We find that there exists a finite coherence even long after the spins become unentangled from each other; this implies that the dephasing rate is slower than the rate in which the spins lose the entanglement Ref. [1].

- [2] G. Catarina and Bruno Murta. Density-matrix renormalization group: a pedagogical introduction. *The European Physical Journal B*, 96(8), August 2023.
- [3] Uma Divakaran and Amit Dutta. The effect of the three-spin interaction and the

- next nearest neighbor interaction on the quenching dynamics of a transverse Ising model. *Journal of Statistical Mechanics: Theory and Experiment*, 2007(11):P11001, 2007.
- [4] E. H. Lieb and D. W. Robinson. The finite group velocity of quantum spin systems. *Commun. Math. Phys.*, 28:251–257, 1972.
- [5] H. Q. Lin. Exact diagonalization of quantum-spin models. *Phys. Rev. B*, 42:6561–6567, Oct 1990.
- [6] Tanay Nag and Amit Dutta. Generation of concurrence between two qubits locally coupled to a one-dimensional spin chain. *Phys. Rev. A*, 94:022316, Aug 2016.
- [7] TANAY NAG, AMIT DUTTA, and AYOTI PATRA. Quenching dynamics and quantum information. *International Journal of Modern Physics B*, 27(01n03):1345036, 2013.
- [8] Tanay Nag, Ayoti Patra, and Amit Dutta. Quantum discord in a spin-1/2 transverse  $xy$  chain following a quench. *Journal of Statistical Mechanics: Theory and Experiment*, 2011(08):P08026, aug 2011.
- [9] Tobias J. Osborne and Michael A. Nielsen. Entanglement in a simple quantum phase transition. *Phys. Rev. A*, 66:032110, Sep 2002.
- [10] Andreas Osterloh, Luigi Amico, Giuseppe Falci, and Rosario Fazio. Scaling of entanglement close to a quantum phase transition. *Nature*, 416(6881):608–610, 2002.
- [11] E. Ovrum and M. Hjorth-Jensen. Quantum computation algorithm for many-body studies, 2007.
- [12] Jiannis K. Pachos and Martin B. Plenio. Three-spin interactions in optical lattices and criticality in cluster hamiltonians. *Phys. Rev. Lett.*, 93:056402, Jul 2004.
- [13] H. T. Quan, Z. Song, X. F. Liu, P. Zanardi, and C. P. Sun. Decay of loschmidt echo enhanced by quantum criticality. *Physical Review Letters*, 96(14), April 2006.
- [14] Subir Sachdev. *Quantum Phase Transitions*. Cambridge University Press, 2 edition, 2011.
- [15] Sebastian Schiffer, Jia Wang, Xia-Ji Liu, and Hui Hu. Many-body localization in  $xy$  spin chains with long-range interactions: An exact-diagonalization study. *Phys. Rev. A*, 100:063619, Dec 2019.
- [16] William K Wootters. Entanglement of formation and concurrence. *Quantum Inf. Comput.*, 1(1):27–44, 2001.